International Journal of Robotics and Control Systems
Vol. 6, No. 1, 2026, pp. 16-35
ISSN 2775-2658
http://pubs2.ascee.org/index.php/ijrcs

Brain Tumor Classification from MRI Images Using Hybrid Deep Learning Approaches: VGG19 with SoftMax and SVM Classifiers

Hanan M. Omran [a,1], Khalil Ibrahim [b,c,2], Gamal T. Abdel-Jaber [a,c,3], Abdel-Nasser Sharkawy [a,d,4,*]

[a] Mechanical Engineering Department, Faculty of Engineering, Qena University, Qena 83523, Egypt
[b] Mechatronics Engineering Department, Faculty of Engineering, Assiut University, Egypt
[c] New Assiut technological university (NATU), New Assiut City, Assiut, 71684, Egypt
[d] Mechanical Engineering Department, College of Engineering, Fahad Bin Sultan University, Tabuk 47721, Saudi Arabia
[1] enghananomran@gmail.com; [2] khalil.ibrahim@aun.edu.eg; [3] gtag2000@eng.svu.edu.eg;
[4] abdelnassersharkawy@eng.svu.edu.eg
[*] Corresponding Author

ARTICLE INFO

Article history
Received October 04, 2025
Revised November 28, 2025
Accepted December 11, 2025

Keywords
Brain Tumor Classification;
Deep Learning Architecture;
Hybrid Model;
VGG19;
SVM-RBF;
Magnetic Resonance Imaging;
Feature Extraction

ABSTRACT

Brain tumor classification from MRI images remains a challenging task due to the complex structure and visual similarity among tumor types. Many existing deep learning models achieve high training accuracy but often suffer from limited generalization on small medical datasets. The VGG19 convolutional neural network for feature extraction and a Support Vector Machine (SVM) classifier with a Radial Basis Function (RBF) kernel are integrated in this study's hybrid deep learning architecture to close this gap. The rationale behind this combination is that VGG19 efficiently captures deep hierarchical image features, while SVM-RBF enhances nonlinear decision boundaries and improves robustness against overfitting. The suggested models were trained and verified using a publicly available brain MRI dataset from Kaggle, which consisted of 7023 contrast-enhanced pictures divided into four classes: glioma, meningioma, pituitary tumor, or no tumor. To guarantee a fair assessment, the data were split into subgroups for testing, validation, and training. According to experimental findings, the VGG19-SVM (RBF) model attained 96.2% validation and 97.8% testing accuracy, whereas the VGG19-Softmax model earned 99% training accuracy and 98.4% validation accuracy. The novelty of this work lies in providing a controlled and systematic comparison between two classification pipelines—VGG19 with Softmax and VGG19 with SVM (RBF)—under identical preprocessing, augmentation, and evaluation settings. Unlike prior studies that report single-model performance, this study analyzes stability, misclassification patterns, and class-wise behavior in a unified experimental framework, offering deeper insight into the conditions under which each model performs best. Images are immediately compressed by the system using AWS Lambda, S3, IAM, CloudWatch, and Docker. Strong stability and steady convergence over time were demonstrated by both models. Comparative analysis confirms that the proposed hybrid architecture provides competitive performance with improved class separation, highlighting its potential for reliable and automated brain tumor diagnosis in clinical settings.

1. Introduction

Brain tumors are a serious medical issue caused by cells growing uncontrollably in or around the brain. Because the brain is in a tight space inside the skull, this growth can press on important areas and affect how the brain works. These tumors can be either non-cancerous or cancerous, but both types can put pressure on the brain and cause problems with thinking, sensing, and moving [1]–[3]. Despite advancements in surgical and therapeutic approaches, accurate and timely diagnosis continues to be a key factor in determining patient outcomes. For the diagnosis of brain tumors, magnetic resonance imaging (MRI) has emerged as the gold standard, as it offers detailed visualization of tumor structure, blood supply, and surrounding tissue issues, aiding physicians in treatment planning. However, Reliable automated methods are necessary since manual MRI scan interpretation is laborious, subjective, and causes observer variability. In order to compress images as soon as they are uploaded, this study introduces a serverless image compression system that uses Amazon Web Services (AWS), combining AWS Lambda, S3, IAM, CloudWatch, and Docker. The system concentrates on tumors of the brain and central nervous system (CNS). Lung and breast cancers are the most common, accounting for 12.4% and 11.5% of all cases, respectively, followed by colorectal (9.6%) and prostate (7.3%) cancers. Brain and CNS tumors, though representing only 1.6% of total cases, have a disproportionately severe clinical impact due to their critical location and complex treatment needs. These findings highlight the ongoing necessity for advanced diagnostic tools and automated systems to improve patient outcomes and early diagnosis. Fig. 1 shows how many new cancer cases happen in different parts of the body around the world, with the percentage of each type of cancer compared to others.

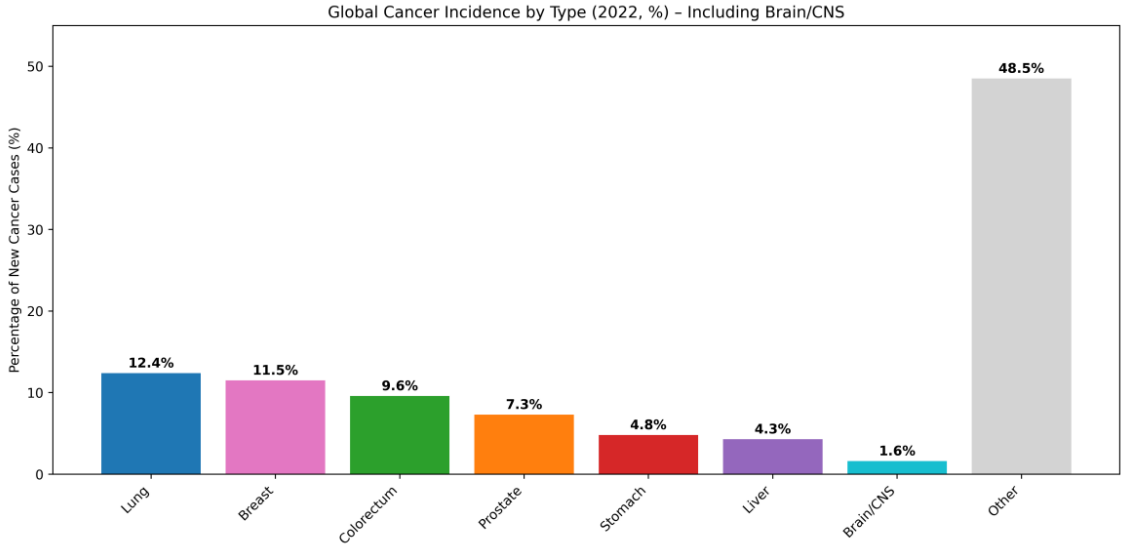

Fig. 1. Global Cancer Incidence Distribution according to (GLOBOCAN 2022)

Artificial intelligence (AI) [4] and machine learning (ML) [5], [6] have become powerful tools in analyzing medical images, allowing for quick and consistent detection and outlining of tumors [7]–[9]. Deep learning (DL) [10]–[13], Convolutional Neural Networks (CNNs) in particular have demonstrated a remarkable capacity to learn discriminative and hierarchical features from MRI data without the requirement for manually created features. However, overfitting and lack of generalization continue to be recurrent problems with current deep learning architectures when they are applied to small or heterogeneous medical datasets. Thus, frameworks that can preserve model robustness across a variety of MRI images while maintaining high diagnostic accuracy are required from a clinical and computational standpoint.

The Visual Geometry Group at Oxford University created the VGG19 architecture, a well-known CNN model [14] that has shown remarkable performance in a variety of computer vision tasks because

of its deep layered structure can extract complex spatial characteristics [15]–[17]. Transfer learning techniques further enhance its utility by allowing pretrained weights from large datasets such as ImageNet to be fine-tuned for medical imaging applications. Even though VGG19's SoftMax classifier works well on large-scale tasks, it might not be the best at handling tiny sample sets or non-linear class boundaries, which are common in medical data. The current study suggests VGG19 and a Support Vector Machine (SVM) classifier using a Radial Basis Function (RBF) kernel are combined in this hybrid deep learning architecture. for deep feature extraction to overcome these constraints [18]. For multiclass brain tumor identification from MRI scans, this integration seeks to increase classification accuracy, improve generalization, and give a more solid decision border. The suggested study contributes to a balanced approach to automated brain tumor classification by bridging the gap between clinical diagnostic requirements and computational efficiency.

While VGG19 or CNN features paired with SVM classifiers have been used in several earlier research studies for brain tumor classification [19]–[21], These studies usually assess a single pipeline and do not have a cohesive experimental setting for direct comparison. In contrast, this study adopts a standardized preprocessing and augmentation strategy and evaluates both VGG19-Softmax and VGG19-SVM under identical conditions. This enables a more rigorous assessment of classifier behavior, stability, and class-specific performance, thereby addressing a gap in prior literature.

1.1. Related Work

In this section, we discuss previous work on the use of VGG 19 and VGG 19-SVM in detecting brain tumors. Artificial intelligence is the field that focuses on building robots that can learn on their own without assistance from humans. Machine learning has made it possible to create machines that think and learn from experiences, similarly to people. Convolutional neural networks, particularly artificial neural networks, a subset of deep learning techniques, are inspired by the natural visual perception mechanism of living organisms. CNNs are multilayered neural networks stacked. Gu et al. (2018) [22] indicated that the three primary types of layers are fully connected, pooling, and convolutional. The width, height, and depth of the input image are the input parameters. The input layer is the initial layer of any CNN model. The number of filters, filter window size, stride, padding, and activation are the parameters of convolutional layers, which are defined right after the input layer. Convolutional layers extract meaningful feature maps for the input location are extracted using convolutional layers by the weighted total is calculated. The output is then created by adding bias after each feature map has been run through an activation function (Kunhoth et al., 2019; Szegedy et al., 2016) [23], [24].

Nielsen (2015) [25] stated that the activation function approach usually uses the rectified linear unit (ReLU) activation. Pooling layers reduce the size of the output from the convolutional layers. When the number of filters in the convolutional layer increases along with the model's size, the output dimensionality furthermore rises at an exponential rate, making it challenging for computers to manage. Pooling layers simplify processing and sometimes reduce noise. There are various types of pooling layers, including maximum pooling, average pooling, global average pooling, and spatial pooling. A max pooling layer is the most widely used pooling layer (Sarigül et al., 2019) [26].

Fakhrou et al., (2021) [27] showed that the output is flattened and fed into a fully linked layer to form a single-array feature vector. Finally, a classification layer is defined using activation functions such as sigmoid, softmax, and tanh. The classification layer creates class scores by combining the retrieved data and determining the number of classes. To standardize learning and reduce training time, batch normalization layers are either placed after the input layer or after the activation layers. Additionally, the loss function is a crucial factor (Ioffe & Szegedy, 2015) [28]. Additionally, the loss function is a crucial factor. The learning process is improved by returning the loss to the CNN model at the end of each epoch (Zhao et al., 2015) [29].

Small datasets rarely benefit from deep convolutional neural networks because of the risk of overfitting inherent in these models. Shu, M. (2019) [30] applied a modified deep neural network to a small dataset that we offer. The research also addresses the implications of our results. CNN is the

classifier in our method, which uses the VGG16 architecture. Sowrirajan et al. (2023) [31] tested the performance of their suggested approach on the VGG16 dataset and calculated its F-score, accuracy, and recall to evaluate its efficacy, obtaining 97.90% classification accuracy for a BT by using the discrete cosine transform technique and k-means to split the dataset, transfer learning to extract features, and ELM to classify tumors.

One of the most well-known deep networks in computer vision, the VGG19 network, was created alongside the VGG16 network. The Visual Geometry Group at Oxford University created it. Three fully connected layers and sixteen convolutional layers make up the network's 19 layers. It can extract complicated and delicate characteristics from photos because of its small-scale (3x3) filters with increasing depth. The fundamental tenet of VGG19 is that the model's capacity to identify visual patterns is enhanced by increasing the depth and number of layers. In terms of computing, it's not the lightest network, but it is extensively employed as a feature extractor or as a backbone model in numerous medical applications, including the detection of brain tumors from magnetic resonance imaging (MRI), where it helps with image analysis and the extraction of distinguishing features that support an automated and precise diagnosis process (Simonyan & Zisserman, 2014) [32].

Sajjad et al. (2019) [15] employed two streams—a 7x7 field for local feature extraction and a 13x13 field for global feature extraction—to segment the tumor using input Cascade CNN. He used rotation, skewness, flipping, and shearing for major data augmentation, VGG19 for cancer grade classification, and a transfer learning method for pattern recognition. Latif et al. (2022) [19] used a 17-layer CNN to extract features before categorizing tumors using a variety of machine learning classifiers, such as SVM, MLP, NB, and RF; SVM produced the best classification results. Senan et al. (2022) [20] employed AlexNet, ResNet18, AlexNet with SVM, and ResNet18 with SVM models to classify the tumour grade after applying min–max normalization before feature extraction.

Vadhnani & Singh (2022) [33] used principal component analysis to reduce the extracted features, the discrete wavelet transform algorithm for feature extraction and Otsu thresholding for tumor segmentation, and SVM for classifying tumor types. Bodapati et al. (2022) [34] employed a median filter on the segmented tumor data after initially segmenting the tumours from MR images using k-means clustering, and then upgraded SVM to classify BT. Rajinikanth et al. (2020) [21] identified BT using multiple classifiers, such as VGG19, linear SVM, and kernel SVM, after customizing the pre-trained VGG19 model using serially fused deep features and handcrafted features. Çınar et al. (2022) [35] applied rotation, shifting, and scaling techniques to supplement the data. Following the augmentation, they used number of DL models for tumor classification in addition to transfer learning for feature extraction from MR images and VGG19.

1.2. Contributions of Current Work

This study introduces a hybrid deep learning framework, referred to as VGG–SVM, designed for efficient and accurate brain tumor (BT) classification from MRI images. While previous studies have utilized Convolutional Neural Networks (CNNs) and Support Vector Machines (SVMs) independently, the present work explores their integration to exploit the complementary strengths of both methods. The robust nonlinear decision boundary of SVM (RBF kernel) is paired with the deep hierarchical feature extraction capacity of VGG19 to improve classification reliability and reduce overfitting on sparse medical data. The following is a summary of this study's primary contributions:

1) To extract deep features from MRI brain tumor images, we use a pre-trained VGG19 architecture that has been fine-tuned to capture discriminative spatial and textural representations pertinent to tumor kinds.
2) Using a Soft-Margin RBF kernel, the retrieved high-level features are flattened and fed into a nonlinear SVM classifier, improving model generalization and allowing for better distinction across overlapping tumor types.
3) The suggested hybrid VGG–SVM model outperforms traditional CNN–Softmax frameworks with a peak accuracy of 97.6%, according to a thorough experimental evaluation. A comparison

analysis with comparable studies confirms the stability and robustness of the suggested strategy across several trials, providing additional support for the results.

This study postulates that, in comparison to standalone CNN classifiers, combining deep hierarchical feature representations from VGG19 with the kernel-based discrimination capability of SVM (RBF) can result in statistically significant improvements in classification accuracy and generalization performance. The main experimental goal of the current effort is to test this idea.

2. Materials and Methods

Several standard and customized Deep Learning Architectures (DLAs) have been proposed in the literature to detect anomalies in medical images [36]–[38]. A novel architecture's development, training, testing, and validation frequently call for a significant amount of computational work and meticulous parameter optimization. To solve particular issues with disease detection, the majority of recent research has modified already-existing, verified DLAs. Prior understanding of an architecture's structure, implementation complexity, tuning techniques, and validation protocols is also necessary for choosing the right one [36], [37], [39]. The three main stages of the framework are shown in Fig. 2: feature extraction using a deep learning model, classification, and pre-processing of the data collection.

We used a transfer learning strategy in this study with the VGG19 model as the primary feature extractor to classify brain tumors from MRI images, three primary steps make up the suggested framework, which is depicted in Fig. 2: (1) data preprocessing and augmentation; (2) deep feature extraction using the VGG19 network; and (3) classification using a Support Vector Machine (SVM) with a Radial Basis Function (RBF) kernel. This combination increases classification accuracy and decreases overfitting by utilizing the SVM's capacity to create nonlinear decision boundaries and the VGG19's capacity to extract rich spatial features.

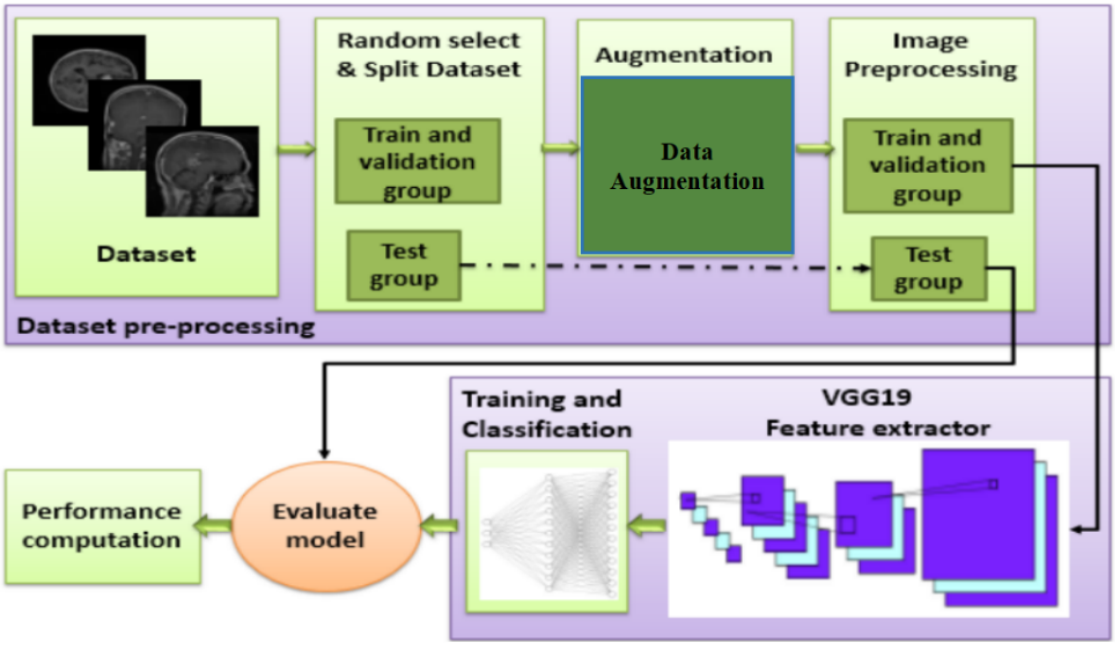

Fig. 2. Stages of the used methodology [40]

TensorFlow and Keras libraries were used to run the experiments in Kaggle with the following configuration: batch size = 32, learning rate = $1 \times 10^{-}3$, optimizer = Adamax, and dropout = 0.25–0.30. To avoid overtraining, early halting was used with a patience of seven epochs. An NVIDIA Tesla P100 GPU and 16 GB of RAM powered the machine. The procedures for detecting and

classifying the brain tumors are depicted in Fig. 3, which begin with input MRI images and end with tumour classification using the two classifiers, Softmax and SVM.

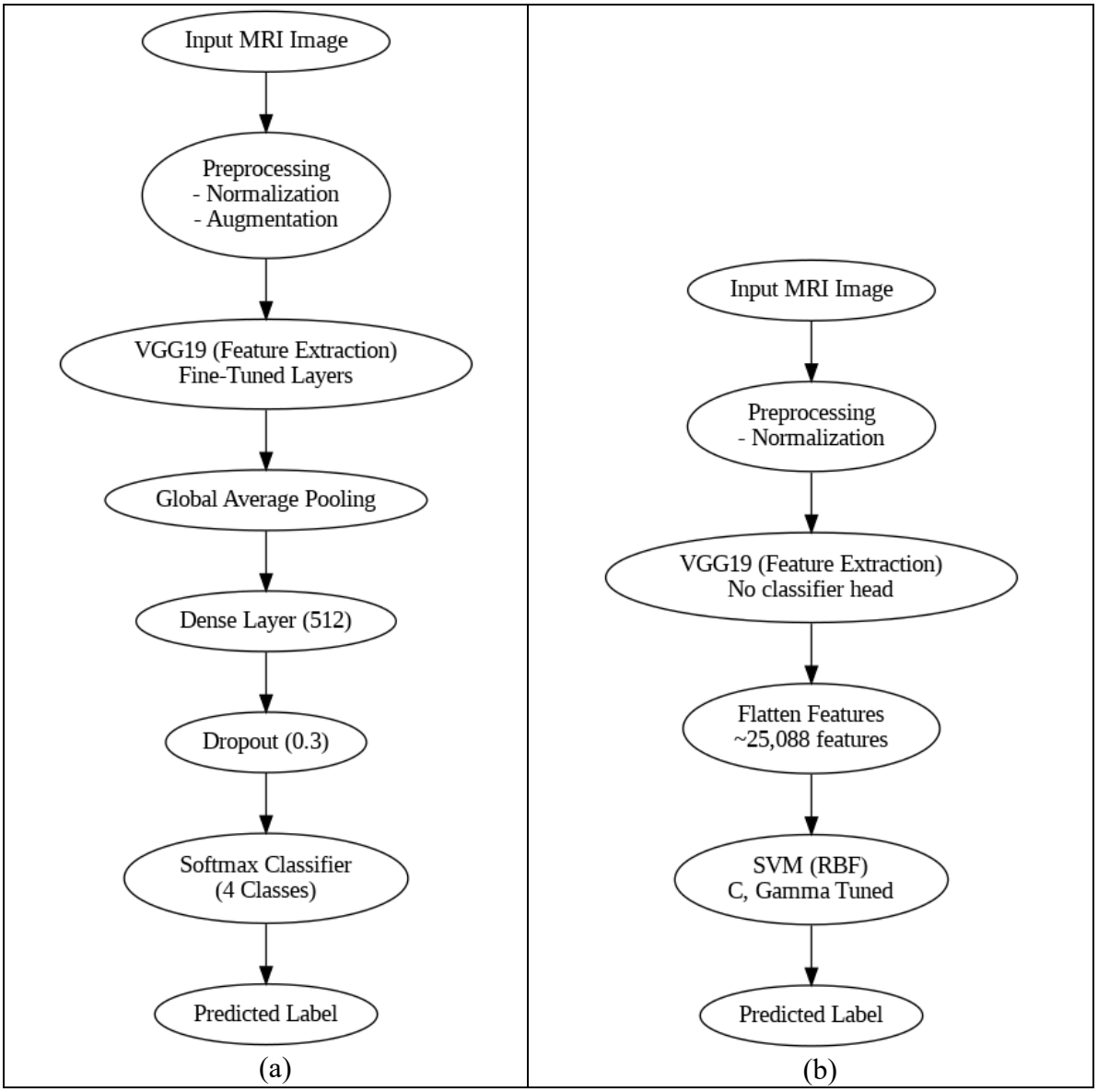

Fig. 3. Procedures for brain tumor classification using: (a) VGG19-softmax; (b) VGG19-SVM

2.1. Collected Dataset

The dataset used in this study was obtained from MRI images from Kaggle website [41], which included 7023 MRI images of four different types of brain tumors: glioma, meningioma, pituitary, and no tumor. Fig. 4 and Fig. 5 depict the distribution of images across categories during the training and testing periods, respectively. Whereas Fig. 6 displays representative MRI images from the dataset.

All images were normalized (rescaled to [0, 1]) and resized to 224 × 224 pixels before to training in order to conform to VGG19's input format. Data augmentation techniques like rotation (±20°), width/height shifting (10%), zooming (up to 20%), horizontal flipping, and brightness modulation (0.8–1.2) were used to further expand the dataset, which was almost balanced between the four classes.

The augmented dataset was divided into 80% training and 20% testing subsets, ensuring stratified sampling for all tumor categories. Although cross-validation was not applied, the validation set was used to monitor model generalization during training and to fine-tune hyperparameters.

All architectural figures were created and adapted from the original VGG19 model proposed by Simonyan and Zisserman (2014) [32], with modifications to reflect the hybrid integration framework applied in this study.

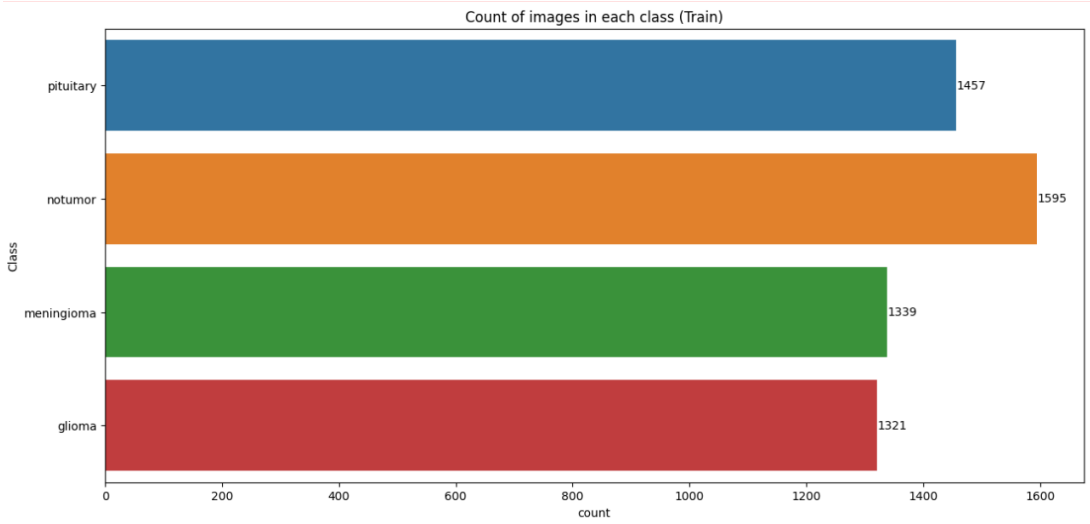

Fig. 4. Number of images for each category at the training stage

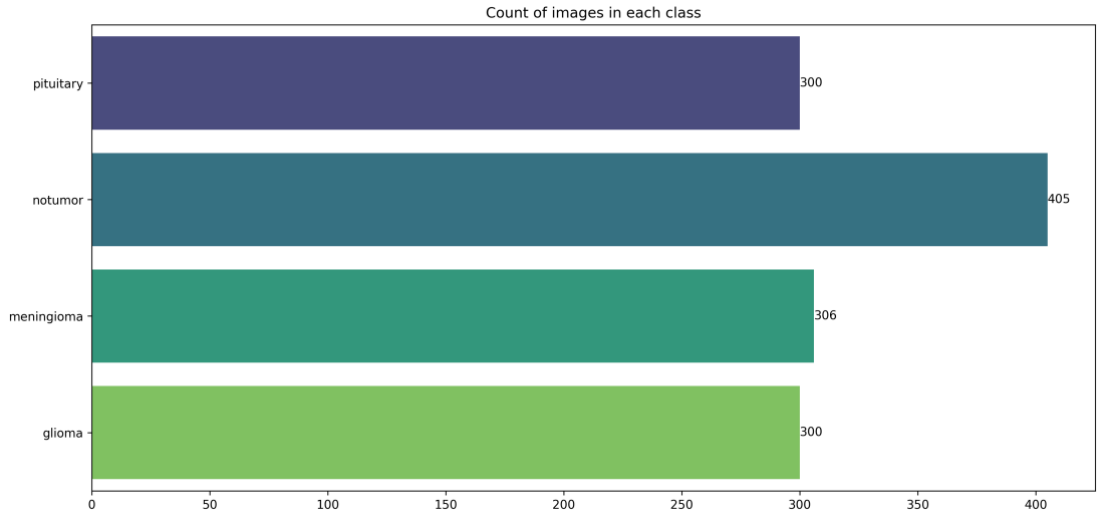

Fig. 5. Number of images for each category in the testing stage

2.2. VGG Network-Softmax Model

This network is shown in Fig. 7. The design uses a fixed-size 224 × 224 × 3 image as its input. A stack of convolutional layers is applied to the image, with each filter being 3 × 3 with stride one and identical padding. Max-pooling, which is carried out over a 2 × 2-pixel window with stride 1, comes after some of the convolutional layers. Following convolutional layers are three fully connected layers: a soft-max layer with 1000 channels comes after the first two, each of which has 4096 channels that are VGG16 [32]. Although it performs nearly as well as VGG16, VGG19 is an even deeper version of the VGG network. This network's primary drawback is the sheer volume of parameters (around 138 million). In the suggested model Convolutional layers and max pooling layers that were previously trained on the ImageNet database were used to extract unique features from brain tumor images, which is built on the VGG19 architecture as a base network. Deep and effective representations of images, including edges, features, and intricate patterns, can be extracted by these layers. To adjust the model to the current classification job (four kinds of brain tumors: meningioma, glioma, pituitary tumor, and non-tumor), a few custom layers were then added. Among these is

Maxpooling, which reduces data size while maintaining the most crucial information by converting 3D feature maps (7×7×512) to a 1D vector (512). Data should be flattened before being entered into dense layers. A fully linked layer that learns high-level patterns unique to the classification task is added using Dense (256, ReLU). The purpose of dropout (0.25) is to enhance generalization and lessen the possibility of overfitting. Images are categorized into four primary classes using the Dense (4, Softmax) output layer. The model can diagnose brain tumors more accurately while lowering the possibility of mis generalization by combining the power of VGG19 in feature extraction with extra layers devoted to classification.

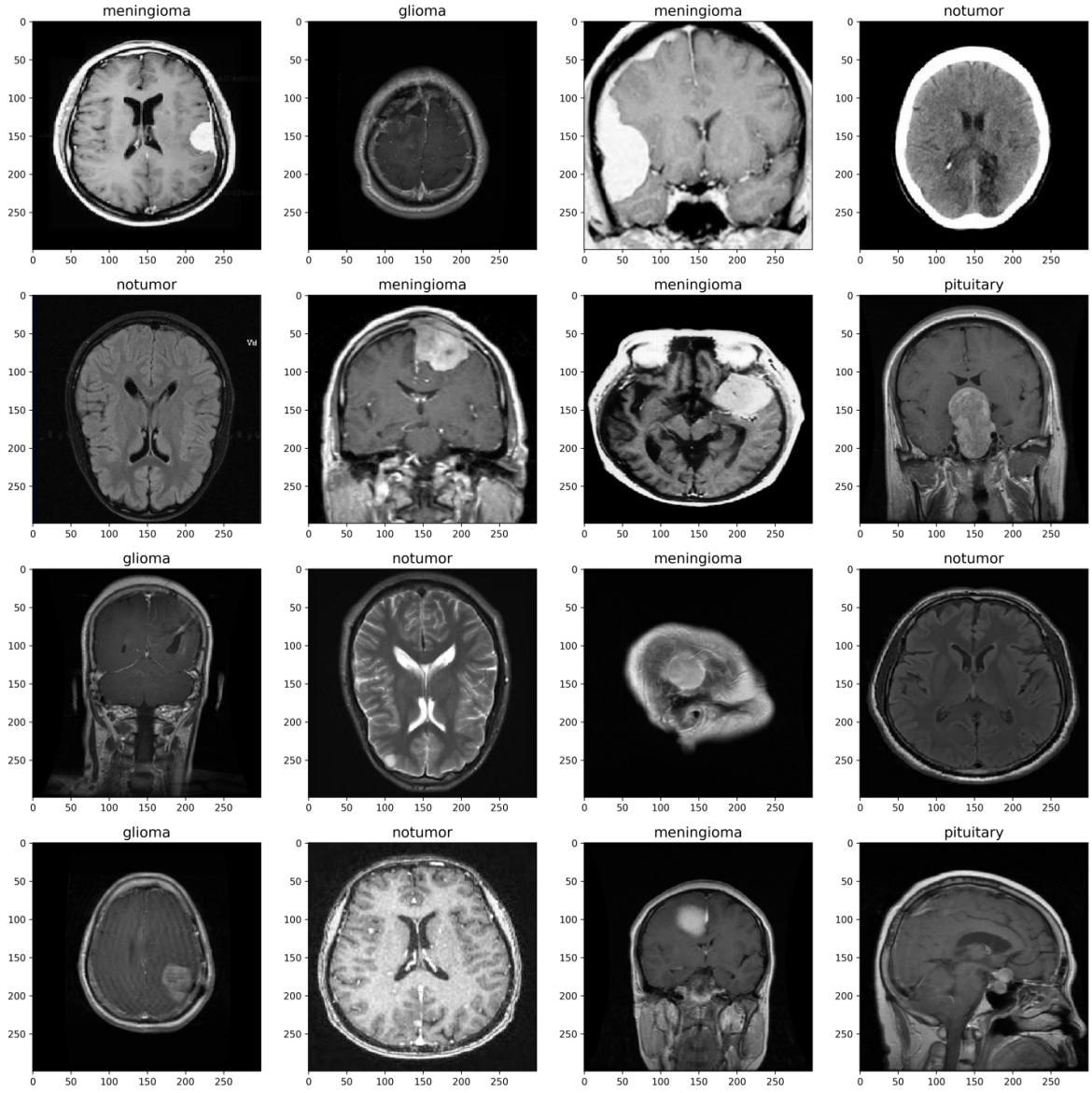

Fig. 6. Examples of dataset samples

2.3. VGG19 - SVM (Soft Margin, RBF Kernel) Model

The VGG19-SVM model combines the strength of SVM as a classification technique with the deep feature extraction capabilities of VGG19 from magnetic resonance imaging (MRI). This model is shown in Fig. 8. High-resolution patterns and features are extracted from brain tumor images using VGG19, a 19-layer deep neural network (Convolution + Pooling + Fully Connected), which eliminates the requirement for human feature construction. A SVM classifier then takes the role of the

conventional Softmax layer in VGG19. A Soft Margin SVM with an RBF kernel determines the best borders between several classes (Glioma, Meningioma, Pituitary, No Tumor).

While the RBF kernel aids in handling intricate nonlinear interactions between extracted features, the soft margin technique permits some minor errors to be accepted, resulting in a more flexible model and improved generalization. The accuracy of this dual architecture (VGG19 + SVM) is frequently higher than that of softmax alone, particularly in challenging medical picture classification tasks where class distinctions are extremely fine.

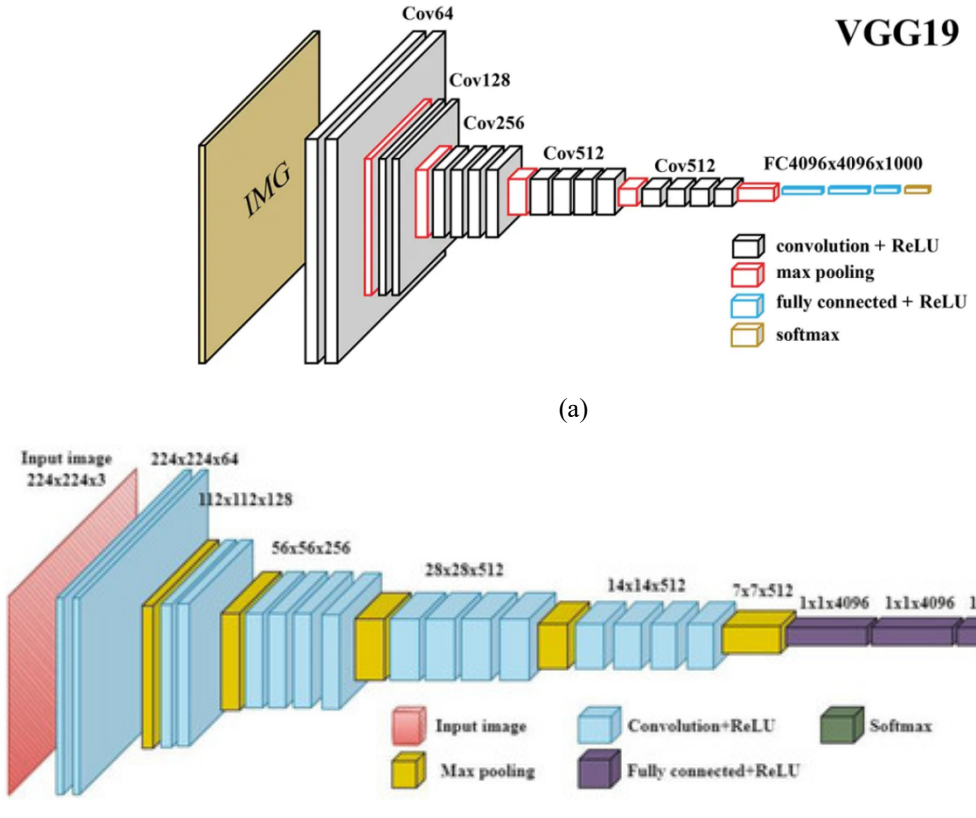

Fig. 7. Architectures of the initial VGG19-SoftMax with two visualizations [42]

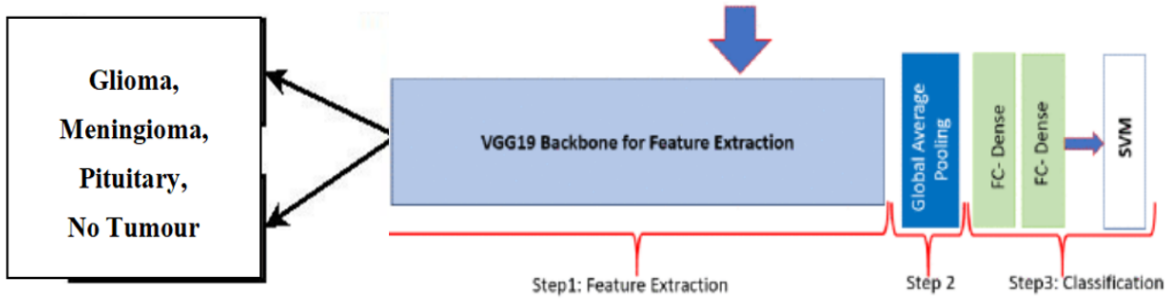

Fig. 8. VGG19 with SVM vector model for classification and feature extraction [43]

2.4. Extraction of Features

The MRI characteristics are extracted using VGG model variations. Features are crucial details pertaining specific task. Features for MRI image processing include an image's texture, shape, border, and intensity value. Only a small percentage of the vast number of variables in large datasets are

crucial for the given job. The separation of the most crucial information is known as feature extraction. In this instance, the retrieved features are the tumor's attributes, including its shape, area, and circularity. The fully linked layer of VGG models is used to extract the features. Because of its deep nature and use of the smallest receptive filters (3×3) with a stride of 1, we have chosen the VGG model for feature extraction. VGG19 offers a notable performance difference among the range of VGG models.

2.5. Classification

A Softmax layer was utilized in the last step of the classification process after the VGG19 network was utilized as a tool to extract characteristics from brain MRI images. Each value indicates the likelihood that a picture belongs to a given class (e.g., glioma, meningioma, pituitary tumor, or no tumor). The Softmax layer converts the final network output into probabilities dispersed over four distinct brain tumor classifications. The model uses the highest probability value to choose the proper image class because the sum of these probabilities equals one. The second type of classification method used in the research is SVM. Since there is non-linear BT data in the form of MR images, we have chosen to apply non-linear SVM. The current paper has implemented SVM with soft edges to discuss every option for raising the categorization accuracy. To determine the final tumor classification, the non-linear SVM was fed with RBF the characteristics that were derived from each VGG model. Table 1 shows the hyperparameters for the VGG and SVM.

Several values of the SVM regularization parameter C (1, 10, 50, 100) were empirically tested, and C = 100 provided the best validation accuracy and most stable decision boundaries. Dimensionality reduction techniques such as PCA were not applied because preserving the full spatially encoded deep feature representation yielded better class separability in preliminary trials. The high dimensionality did not introduce overfitting due to the sufficiently large dataset and the regularization behavior of the RBF kernel

Table 1. Hyperparameters for VGG19 and SVM (with RBF kernel)

Model	Hyperparameter	Value / Setting
VGG19	Input image size	224 × 224 × 3
	Batch size	32
	Learning rate	0.001
	Optimizer	Adams
	Epochs	100
	Dropout rate	0.25 (on fully connected layers)
	Activation function	ReLU (hidden), Softmax (output)
SVM	Kernel function	RBF (Radial Basis Function)
	Regularization (C)	100
	Gamma	scale (or tuned via cross-validation)
	Decision function	one-vs-rest (OvR)

2.6. Performance Evaluation Metrics

True positive (TP), true negative (TN), false positive (FP), and false negative (FN) are used in medical image processing and learning to assess the effectiveness of categorization models. A true positive is a model that properly and error-free detects an illness, meaning it correctly recognizes a competitor when one is present. The phrase "True Negative" describes situations in which the model correctly identifies the lack of a tumor when the image is genuinely benign, demonstrating the model's ability to prevent false positives. False Positives, on the other hand, occur when the model incorrectly identifies a benign image as having a tumor. Errors of this kind might cause patients to feel anxious and undergo needless examinations.

Although false negatives are the most dangerous possible mistake, the model may mistakenly classify them as benign, missing a true illness and postponing diagnosis and treatment. Because they directly affect patient safety, lowering false negatives is much more crucial in medical applications, while lowering false positives helps the medical system function more efficiently by cutting down on

pointless testing. Metrics like accuracy, recall, and F1-score are commonly computed to assess a model's overall performance based on these ideas. These measures show how well the model balances preventing false alarms with detecting actual illness conditions. Fig. 9 show the confusion matrix parameters [44]–[46].

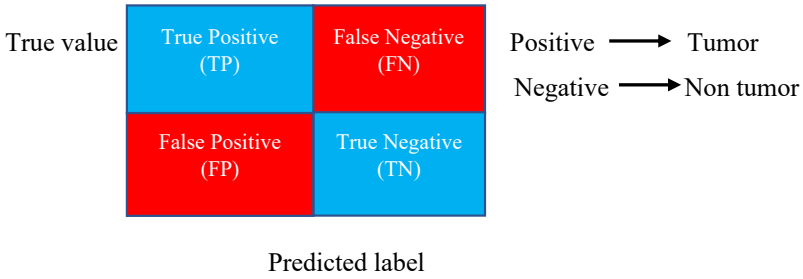

Fig. 9. Confusion matrix parameters

The parameters of the confusion matrix are discussed as follows:

- TP (True Positive): The model detected the tumor when it was actually present.
- TN (True Negative): The model confirmed that the case was benign when it was actually benign.
- FP (False Positive): The model alerted to the presence of a tumor when the image was benign.
- FN (False Negative): The model ignored the tumor and considered the case benign.

The testing set was subjected to the trained model, and performance metrics were computed using the model's predictions. The study employed scoring measures. The following is how it depicts these measures: Sensitivity or recall was defined as the proportion of all affirmative groups that had the correct forecast. Increasing the sensitivity improved the performance of the trained model.

$$\text{Sensitivity} = \frac{TP}{TP + FN} \tag{1}$$

A classification model's ability to identify negative cases was assessed using its specificity. A high specificity indicates that the model successfully identified negative cases and had minimal false positives.

$$\text{Specificity} = \frac{TN}{TN + FP} \tag{2}$$

The precision metric assessed how well the model predicted the results for each class. The model performed better the more precisely it was instructed.

$$\text{Precision} = \frac{TP}{TP + FP} \tag{3}$$

The F1-score was used to assess the model's accuracy in identifying pertinent elements without missing too many and without include irrelevant ones. The trained model performed better when the F1-score was higher.

$$\text{F1} - \text{score} = \frac{\frac{TP}{TP+FP} \times \frac{TP}{TP+FN}}{\frac{TP}{TP+FP} + \frac{TP}{TP+FN}} \tag{4}$$

3. Results and Discussion

3.1. Experimental Results

The results from the suggested models are shown in this part, along with a discussion of their importance in relation to brain MRI classification. The objective was to assess how well the system was built to identify between four categories: glioma, meningioma, pituitary tumour, and no tumor. The training-validation procedure, model performance measures, and a comparison of the VGG19–Softmax and VGG19–SVM (RBF) architectures are all included in the experimental evaluation.

7023 T1-weighted contrast-enhanced MRI images, evenly distributed among the four categories, made up the dataset used for the tests. The VGG19 model's training and validation curves for accuracy, loss, precision, and recall are displayed in Fig. 10. A smooth convergence tendency was confirmed by the continuous improvement in accuracy and decrease in loss as the number of epochs grew. As confirmed by early stopping, the convergence points shows that the model successfully learnt discriminative features without exhibiting significant overfitting

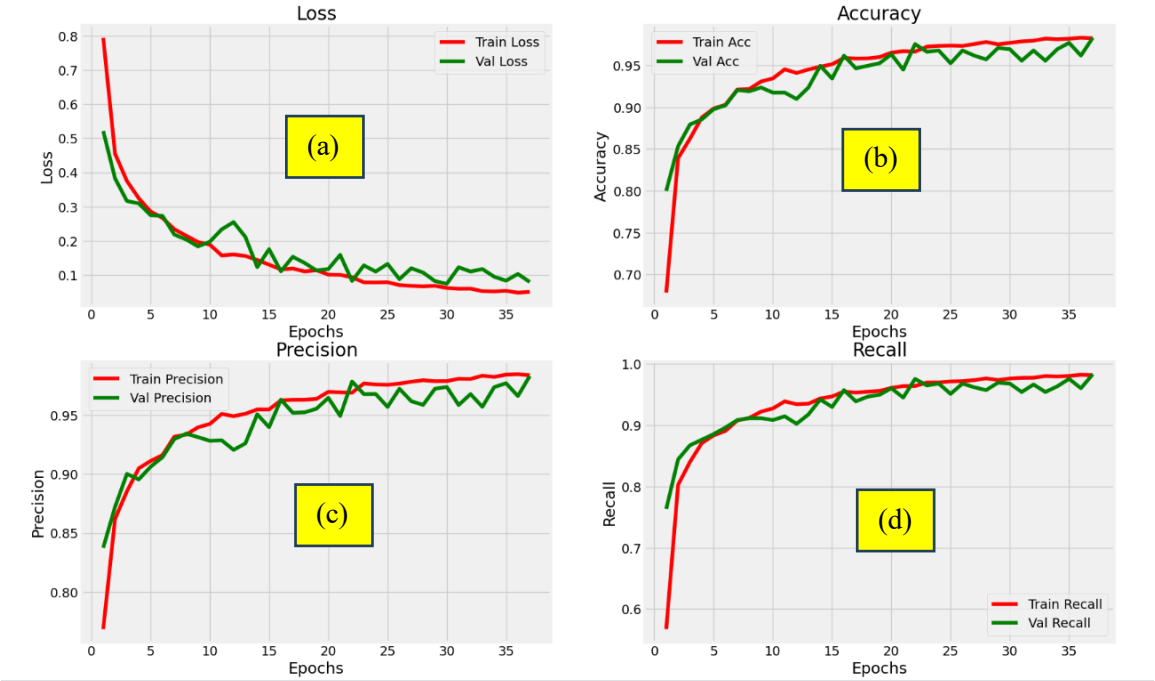

Fig. 10. Convergence of training and validation process: (a) Loss; (b) accuracy; (c) precision; (d) recall

The models' categorization performance is shown by the confusion matrices in Fig. 11–(a) and Fig. 11–(b). The VGG19 model performed exceptionally well in the no-tumor and pituitary categories, both achieving 100% recall, with an overall accuracy of 97.1% (637/656). The majority of minor misclassifications were found between meningioma and pituitary, most likely as a result of overlapping visual patterns in MRI intensities. While VGG19 alone performed better in glioma and pituitary predictions, the SVM-RBF classifier performed slightly better in meningioma and no-tumor instances, achieving an overall accuracy of 97.4% (639/656). Fig. 12 illustrates the close performance of both models across all tumour types by comparing them in terms of precision, recall, and F1-score.

VGG19 with Softmax demonstrated outstanding convergence and 27eneralization in numerical evaluation, achieving validation and testing accuracies of 98.40% and 97.80%, respectively. However, smaller or less varied datasets may reduce the model's adaptability, increasing the likelihood of overfitting. In contrast, VGG19 with SVM (RBF) showed stronger 27eneralization on unseen data but slightly lower accuracy (97.4%). This is probably because the SVM's regularization parameters (C and γ) better govern decision boundaries when data are scarce. While Table 2 lists the advantages and disadvantages of VGG19 and SVM RBF and comparison between them.

These results are consistent with previous research by Sajjad et al. (2019) and Latif et al. (2022), which also noted the advantages of integrating CNN feature extraction with external classifiers like SVM for better brain tumour diagnosis. In contrast to earlier research, our system uses structured augmentation and fine-tuning of VGG19's upper convolutional blocks, which increases stability across categories.

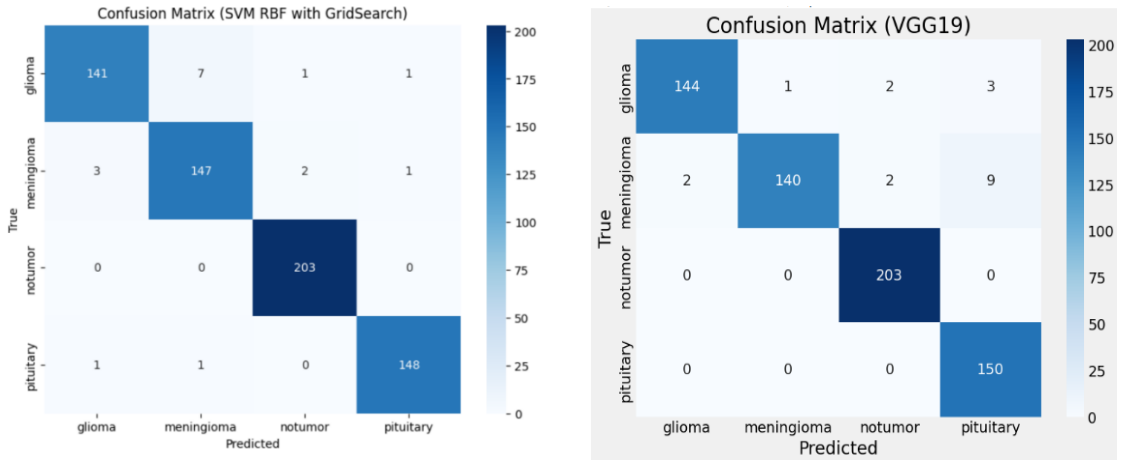

Fig. 11. Analysis of the confusion matrix: (a) VGG 19-SVM RBF model; (b) VGG 19 model

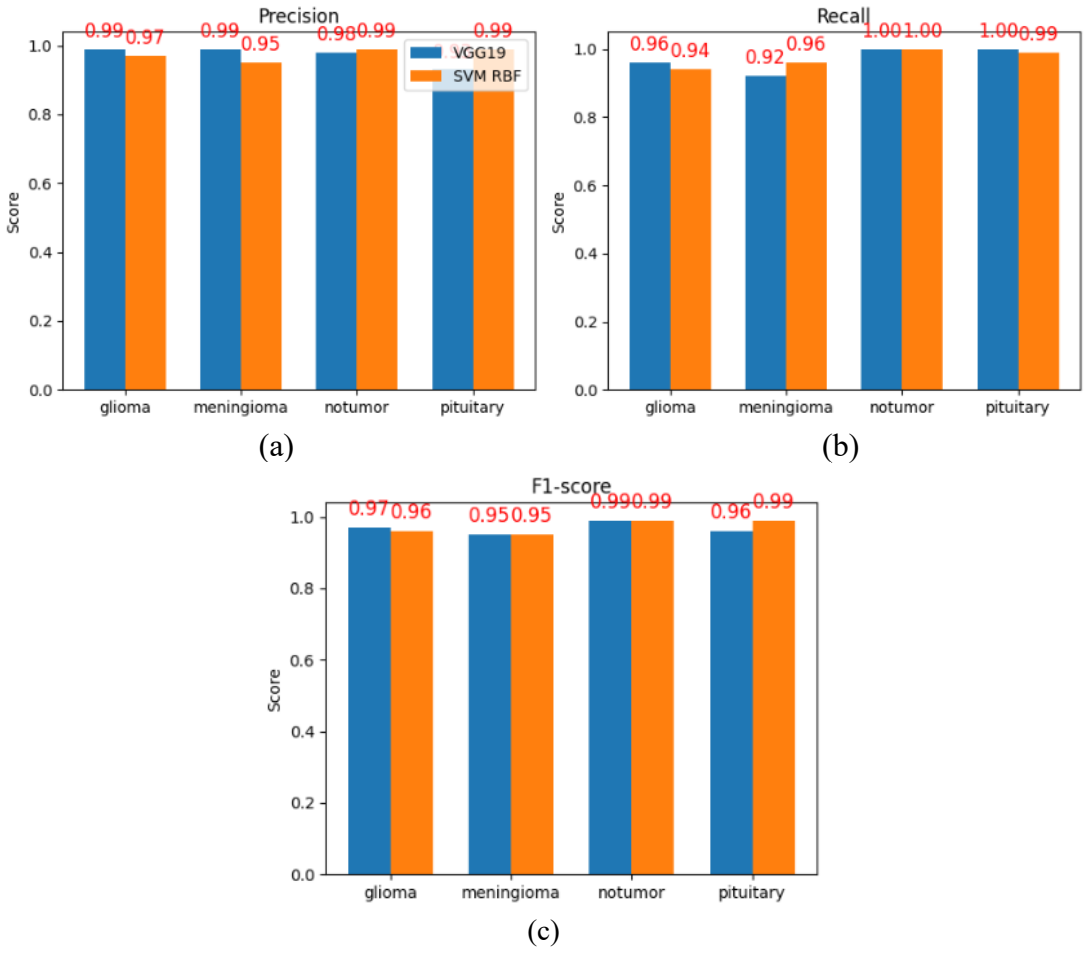

Fig. 12. Comparison of VGG19 vs SVM RBF: (a) Precision; (b) recall; (c) F1-score

It is important to recognize certain limits in spite of these impressive outcomes. Initially, no cross-dataset or external benchmarking was done; instead, the models were trained and verified on a single public dataset (Kaggle MRI). This can limit the data' applicability to different imaging techniques or scanner types. Second, the dataset still has a small amount of class bias that could compromise border precision even though data augmentation helped lessen imbalance. Third, the models' direct clinical use is limited since they are not intrinsically interpretable. Future research could improve interpretability and aid in radiological decision-making by utilizing explainable-AI technologies like Grad-CAM or SHAP.

Table 2. Comparison of VGG19 vs SVM RBF

Model	Validation Accuracy	Test Accuracy	Features	Disadvantages
VGG19 + Softmax	98.40%	98.40%	- End-to-end training. - Stable accuracy and loss curves. - Confusion matrix shows the lowest error rate.	- Less flexible if data changes. - May suffer from overfitting in small groups.
VGG19 + SVM (RBF)	96.20%	97.80%	- Robust performance even with limited data. - Clearer decision intervals between classes. - Leverage (C, γ) coefficients for control.	- Slightly lower accuracy than Softmax. - Additional time is required to select the optimal parameters (tuning).

The strong recall values are especially significant from a clinical standpoint since they lower the possibility of overlooking tumour instances, which is crucial for diagnostic applications. However, treatment choices may be affected by even small misclassifications between meningioma and pituitary categories, underscoring the necessity of ongoing feature sensitivity improvement.

Overall, a fair trade-off between accuracy, generalisation, and computing economy was shown by combining VGG19 feature extraction with SVM (RBF) classification. The paper demonstrates that automated brain-tumor classification can be successfully supported by hybrid deep-learning architectures while preserving statistical and interpretative transparency. Table 3 shows the comparison between previous research in brain tumor detection using VGG with different classifier (softmax-SVM-ELM) the results of the current research

Table 3. Comparative analysis of related work in brain tumor classification

Paper	Model Used	Classification Accuracy
[47]	VGG19 + ELM	97.90%
[15]	VGG19	94.58%
[19]	SVM	96.19% for HGG 95.46% for LGG
[20]	AlexNet + SVM, ResNet18 + SVM	95.10% 91.20%
[33]	SVM(RBF) SVM(Linear)	97.60% 94.00%
[34]	K-means + ISVM	95.00%
[21]	VGG19 SVM(RBF) SVM(Linear)	95.90%, 95.30%, 95.60%
Proposed approach	VGG19-SoftMax VGG19-SVM(RBF)	98.40% 97.80%

3.2. Error Analysis and Discussion

The two classification pipelines exhibit different error patterns when the confusion matrices and class-wise findings are examined. The VGG19 + SVM (RBF) classifier showed the highest

misclassification rate between meningioma and pituitary tumors, whereas the VGG19 + Softmax model showed the most confusion between glioma and meningioma. Both classifier-specific decision behaviour and image-level similarities are consistent with these mistake tendencies.

According to earlier research, gliomas and meningiomas can have similar morphological features and overlapping enhancement patterns on T1-weighted contrast-enhanced MRI, which can make it more difficult to distinguish between the two types. Similarly, it might be difficult to differentiate between meningiomas and pituitary tumors in feature space if they have similar intensity profiles or present in physically close areas. These conclusions are consistent with findings from previous studies on medical imaging, which show that CNN-based and SVM-based classification performance can be impacted by minute textural similarities.

The increased glioma–meningioma confusion can be explained by the Softmax classifier, which was trained end-to-end using VGG19 and has a tendency to be sensitive to intra-class variability. On the other hand, margin-based separation is enforced by the SVM (RBF) classifier, which uses fixed deep features. this can improve robustness for some class boundaries but may shift the dominant errors toward categories where features cluster closely (e.g., meningioma vs. pituitary).

The literature has suggested a number of approaches to deal with these class-specific difficulties. By emphasizing discriminative tumour locations, attention processes can dramatically reduce misclassification, according to recent research. CNNs in conjunction with attention modules were shown by Rasheed et al. to enhance the distinction between visually identical brain tumour kinds. Similarly, channel-wise attention improves fine-grained identification of tumours with similar intensity or texture patterns, according to a study published in BMC Medical Imaging (2024) [48]. Decision regions have also been visualized and the reasons for classification failures have been identified using explainable AI approaches, namely Grad-CAM. According to a 2024 PubMed study [49] using Grad-CAM with ResNet50, misclassifications often occur when the model concentrates on non-lesion areas or unclear borders. Furthermore, as mentioned in a recent MDPI study, hybrid architectures that combine CNN feature extraction with SVM decision boundaries are also being investigated; nevertheless, these models may still have trouble with class overlap when the feature vectors are adjacent to one another in high-dimensional space [48]–[50].

Future research could examine a number of enhancements based on these insights:

1) Using ROI-focused training or attention methods to highlight tumor-specific areas [51].
2) Improving feature selection and data preparation using Grad-CAM-based interpretability [52].
3) Applying class-aware training techniques, such as targeted augmentation or focal loss for often confused classes
4) Investigating ensemble or hybrid decision procedures that combine the complimentary advantages of SVM and Softmax classifiers [48].

In conclusion, the intrinsic performance of the corresponding classifiers as well as anatomical commonalities among tumour classifications are responsible for the observed error patterns. Misclassification of closely related tumour types may be greatly decreased by addressing these problems through targeted model improvements.

4. Conclusion and Future Work

Two VGG19-based architectures for automated brain tumour classification using magnetic resonance imaging (MRI) were designed and assessed in this study. While the second model combined VGG19 features with an SVM classifier utilizing an RBF kernel, the first model used a VGG19 + Softmax structure. Throughout the training, validation, and testing stages, both models showed excellent and consistent performance. In particular, the VGG19 + Softmax model demonstrated high learning capabilities and continuous convergence on the provided dataset, achieving validation and testing accuracies of 98.40%. Similar results were obtained by the VGG19 + SVM (RBF) mode

achieved performance with validation and testing accuracies of 96.20 % and 97.80 %, respectively, benefiting from the SVM's flexibility in handling nonlinear class boundaries through regularization parameters (C, γ).

These results suggest that the VGG19 + Softmax model, which offers somewhat greater overall accuracy, is better when there is an abundance of well-distributed training data. On the other hand, when data are scarce or diverse, VGG19 + SVM (RBF) provides a more flexible and reliable solution while preserving a balance between interpretability and accuracy. These findings demonstrate that MRI-based tumour identification can be improved by combining convolutional feature extraction with kernel-based classification.

Even with the positive results, there are still restrictions to be aware of. A single public dataset (Kaggle MRI) was used to train and assess the models, which might not have captured variances from various MRI scanners or acquisition techniques. Additionally, even though data augmentation lessened imbalance, a little amount of class bias still exists, which could affect border precision. Model interpretability is another drawback; deep neural networks' "black-box" characteristics can make clinical validation more difficult. Translating the models into real-world healthcare settings will require addressing these issues.

Future implementation of such systems must guarantee patient privacy, secure data management, and compliance with institutional data governance frameworks from an ethical and practical standpoint. Instead of acting as independent diagnostic agents, AI-assisted tools ought to function as decision-support systems that enhance rather than replace radiologists' knowledge.

The VGG19 + Softmax model showed marginally better accuracy within the parameters of the two pipelines assessed in this work, whereas the VGG19 + SVM (RBF) model showed more flexibility in decision-boundary control. These results are exclusive to the experimental configuration and do not rule out the possible benefits of more modern topologies like ResNet or DenseNet.

Based on the study's results and existing constraints, a number of areas are suggested for further research. To increase the generalizability of the model, MRI images from various sources will first be added to the dataset. Second, to enhance clinical interpretability and visualize feature importance, explainable AI methods as Grad-CAM and SHAP will be investigated. Third, the system can be made more dependable for medical decision-making by including uncertainty quantification techniques to provide confidence levels for every prediction. In order to balance accuracy, flexibility, and resilience in real-world scenarios, hybrid ensemble architectures that combine VGG19 + Softmax and VGG19 + SVM (RBF) in a single framework will be examined.

List of Abbreviations

VGG19	VGG19 is a deep convolutional neural network (CNN) that was developed by the Visual Geometry Group at Oxford University. 19 represents the 19 layers.
SVM	Support Vector Machine.
RBF	Radial Basis Function.
AWS	Amazon Web Services.
CNS	Central Nervous System.
MRI	Magnetic Resonance Imaging.
CNNs	Convolutional Neural Networks.
ReLU	Rectified Linear Unit.
BT	Brain Tumor.

Supplementary Materials: All data is included in the paper.

Author Contribution: All authors contributed equally to this paper. All authors read and approved the final paper.

Funding: This research received no external funding.

Acknowledgment: Not Applicable.

Conflicts of Interest: The authors declare no conflict of interest.

References

[1] M. E. Davis, "Epidemiology and overview of gliomas," *Seminars in Oncology Nursing*, vol. 34, no. 5, pp. 420–429, 2018, https://doi.org/10.1016/j.soncn.2018.10.001.

[2] J. T. Low, Q. T. Ostrom, G. Cioffi, C. Neff, K. A. Waite, C. Kruchko, and J. S. Barnholtz-Sloan, "Primary brain and other central nervous system tumors in the United States (2014–2018): A summary of the CBTRUS statistical report for clinicians," *Neuro-Oncology Practice*, vol. 9, no. 3, pp. 165–182, 2022, https://doi.org/10.1093/nop/npac015.

[3] D. N. Louis, A. Perry, P. Wesseling, D. J. Brat, I. A. Cree, D. Figarella-Branger, C. Hawkins, H. K. Ng, S. M. Pfister, G. Reifenberger, R. Soffietti, A. von Deimling, and D. W. Ellison, "The 2021 WHO classification of tumors of the central nervous system: A summary," *Neuro-Oncology*, vol. 23, no. 8, pp. 1231–1251, 2021, https://doi.org/10.1093/neuonc/noab106.

[4] K. Song and Y. Yan, "A noise robust method based on completed local binary patterns for hot-rolled steel strip surface defects," *Applied Surface Science*, vol. 285, pp. 858–864, 2013, https://doi.org/10.1016/j.apsusc.2013.09.002.

[5] S. Karthikeyan, M. C. Pravin, B. Sathyabama, and M. Mareeswari, "DWT based LCP features for the classification of steel surface defects in SEM images with KNN classifier," *Australian Journal of Basic and Applied Sciences*, vol. 10, no. 5, pp. 13–19, 2016, https://ssrn.com/abstract=2792637.

[6] Q. Luo, Y. Sun, P. Li, O. Simpson, L. Tian, and Y. He, "Generalized completed local binary patterns for time-efficient steel surface defect classification," *IEEE Transactions on Instrumentation and Measurement*, vol. 68, no. 3, pp. 667–679, 2019, https://doi.org/10.1109/TIM.2018.2852918.

[7] A. K. Philip, B. A. Samuel, S. Bhatia, S. A. M. Khalifa, and H. R. El-Seedi, "Artificial intelligence and precision medicine: A new frontier for the treatment of brain tumors," *Life*, vol. 13, no. 1, p. 24, 2022, https://doi.org/10.3390/life13010024.

[8] M. A. Alam, A. Sohel, K. M. Hasan, and I. Ahmad, "Advancing brain tumor detection using machine learning and artificial intelligence: A systematic literature review of predictive models and diagnostic accuracy," *Strategic Data Management and Innovation*, vol. 1, no. 1, pp. 37–55, 2024, https://doi.org/10.71292/sdmi.v1i01.6.

[9] Z. Akkus, A. Galimzianova, A. Hoogi, D. L. Rubin, and B. J. Erickson, "Deep learning for brain MRI segmentation: State of the art and future directions," *Journal of Digital Imaging*, vol. 30, no. 4, pp. 449–459, 2017, https://doi.org/10.1007/s10278-017-9983-4.

[10] X. Feng, X. Gao, and L. Luo, "A ResNet50-based method for classifying surface defects in hot-rolled strip steel," *Mathematics*, vol. 9, no. 19, p. 2359, 2021, https://doi.org/10.3390/math9192359.

[11] Z.-W. Xu, X.-M. Liu, and K. Zhang, "Mechanical properties prediction for hot rolled alloy steel using convolutional neural network," *IEEE Access*, vol. 7, pp. 47068–47078, 2019, https://doi.org/10.1109/ACCESS.2019.2909586.

[12] A. Bouguettaya, Z. Mentouri, and H. Zarzour, "Deep ensemble transfer learning-based approach for classifying hot-rolled steel strips surface defects," *The International Journal of Advanced Manufacturing Technology*, vol. 125, no. 11, pp. 5313–5322, 2023, https://doi.org/10.1007/s00170-023-10947-8.

[13] J. Zhang, X. Kang, H. Ni, and F. Ren, "Surface defect detection of steel strips based on classification priority YOLOv3-dense network," *Ironmaking & Steelmaking*, vol. 48, no. 5, pp. 547–558, 2021, https://doi.org/10.1080/03019233.2020.1816806.

[14] M. Fahmi, A. Yudhana, Sunardi, A.-N. Sharkawy, and Furizal, "Classification for waste image in convolutional neural network using morph-HSV color model," *Scientific Journal of Engineering Research*, vol. 1, no. 1, pp. 18–25, Jan. 2025, https://doi.org/10.64539/sjer.v1i1.2025.12.

[15] M. Sajjad, S. Khan, K. Muhammad, W. Wu, A. Ullah, and S. W. Baik, "Multi-grade brain tumor classification using deep CNN with extensive data augmentation," *Journal of Computational Science*, vol. 30, pp. 174–182, 2019, https://doi.org/10.1016/j.jocs.2018.12.003.

[16] Z. N. K. Swati, Q. Zhao, M. Kabir, F. Ali, Z. Ali, S. Ahmed, and J. Lu, "Brain tumor classification for MR images using transfer learning and fine-tuning," *Computerized Medical Imaging and Graphics*, vol. 75, pp. 34–46, 2019, https://doi.org/10.1016/j.compmedimag.2019.05.001.

[17] S. Deepak and P. M. Ameer, "Brain tumor classification using deep CNN features via transfer learning," *Computers in Biology and Medicine*, vol. 111, p. 103345, 2019, https://doi.org/10.1016/j.compbiomed.2019.103345.

[18] A.-N. Abidin, M. Minhajul, M. Munzir, A. Imantoyo, N. W. B. Grendis, A. S. H. San, A. A. Mostfa, Furizal, and A.-N. Sharkawy, "Classification of heart (cardiovascular) disease using the SVM method," *Indonesian Journal of Modern Science and Technology*, vol. 1, no. 1, pp. 9–15, Jan. 2025, https://doi.org/10.64021/ijmst.1.1.9-15.2025.

[19] G. Latif, G. Ben Brahim, D. N. F. A. Iskandar, A. Bashar, and J. Alghazo, "Glioma tumors' classification using deep-neural-network-based features with SVM classifier," *Diagnostics*, vol. 12, no. 4, p. 1018, 2022, https://doi.org/10.3390/diagnostics12041018.

[20] E. M. Senan, M. E. Jadhav, T. H. Rassem, A. S. Aljaloud, B. A. Mohammed, and Z. G. Al-Mekhlafi, "Early diagnosis of brain tumour MRI images using hybrid techniques between deep and machine learning," *Computational and Mathematical Methods in Medicine*, vol. 2022, p. 8330833, 2022, https://doi.org/10.1155/2022/8330833.

[21] V. Rajinikanth, A. N. J. Raj, K. P. Thanaraj, and G. R. Naik, "A customized VGG19 network with concatenation of deep and handcrafted features for brain tumor detection," *Applied Sciences*, vol. 10, no. 10, p. 3429, 2020, https://doi.org/10.3390/app10103429.

[22] H. Chu, Y. Ji, D. Zhu, Z. Ye, J. Tan, X. Hou, and Y. Lin, "Artificial intelligence in tongue image recognition," *International Journal of Software Science and Computational Intelligence*, vol. 15, no. 1, pp. 1–25, 2023, https://doi.org/10.4018/IJSSCI.328771.

[23] J. Kunhoth, A. Karkar, S. Al-Maadeed, and A. Al-Attiyah, "Comparative analysis of computer-vision and BLE technology based indoor navigation systems for people with visual impairments," *International Journal of Health Geographics*, vol. 18, no. 1, p. 29, 2019, https://doi.org/10.1186/s12942-019-0193-9.

[24] C. Szegedy, V. Vanhoucke, S. Ioffe, J. Shlens, and Z. Wojna, "Rethinking the inception architecture for computer vision," in *Proceedings of the IEEE Conference on Computer Vision and Pattern Recognition*, Las Vegas, NV, USA, 2016, pp. 2818–2826, https://doi.org/10.1109/CVPR.2016.308.

[25] M. A. Nielsen, *Neural networks and deep learning*, San Francisco, CA, USA: Determination Press, 2015, https://books.google.co.id/books?id=STDBswEACAAJ.

[26] M. Sarıgül, B. M. Ozyildirim, and M. Avci, "Differential convolutional neural network," *Neural Networks*, vol. 116, pp. 279–287, 2019, https://doi.org/10.1016/j.neunet.2019.04.025.

[27] A. Fakhrou, J. Kunhoth, and S. Al Maadeed, "Smartphone-based food recognition system using multiple deep CNN models," *Multimedia Tools and Applications*, vol. 80, no. 21, pp. 33011–33032, 2021, https://doi.org/10.1007/s11042-021-11329-6.

[28] S. Ioffe and C. Szegedy, "Batch normalization: Accelerating deep network training by reducing internal covariate shift," *arXiv preprint*, arXiv:1502.03167, 2015, https://doi.org/10.48550/arXiv.1502.03167.

[29] H. Zhao, O. Gallo, I. Frosio, and J. Kautz, "Loss functions for neural networks for image processing," *arXiv preprint*, arXiv:1511.08861, 2018, https://doi.org/10.48550/arXiv.1511.08861.

[30] M. Shu, "Deep learning for image classification on very small datasets using transfer learning," M.S. thesis, Iowa State University, Ames, IA, USA, 2019, https://doi.org/10.31274/cc-20240624-493.

[31] S. R. Sowrirajan, S. Balasubramanian, and R. S. P. Raj, "MRI brain tumor classification using a hybrid VGG16-NADE model," *Brazilian Archives of Biology and Technology*, vol. 66, p. e23220071, 2022, https://doi.org/10.1590/1678-4324-2023220071.

[32] K. Simonyan and A. Zisserman, "Very deep convolutional networks for large-scale image recognition," *arXiv preprint*, arXiv:1409.1556, 2014, https://doi.org/10.48550/arXiv.1409.1556.

[33] S. Vadhnani and N. Singh, "Brain tumor segmentation and classification in MRI using SVM and its variants: A survey," *Multimedia Tools and Applications*, vol. 81, no. 22, pp. 31631–31656, 2022, https://doi.org/10.1007/s11042-022-12240-4.

[34] N. Bodapati, A. Divya, N. Triveni, N. Indiradevi, and K. Yamini, "Brain tumor detection on MR images using improved support vector machine," in *Proceedings of the International Conference on Electronics and Renewable Systems*, 2022, pp. 1022–1029, https://doi.org/10.1109/ICEARS53579.2022.9752093.

[35] N. Çınar, B. Kaya, and M. Kaya, "Comparison of deep learning models for brain tumor classification using MRI images," in *Proceedings of the International Conference on Decision Aid Sciences and Applications*, 2022, pp. 1382–1385, https://doi.org/10.1109/DASA54658.2022.9765250.

[36] A. Gudigar, U. Raghavendra, T. R. San, E. J. Ciaccio, and U. R. Acharya, "Application of multiresolution analysis for automated detection of brain abnormality using MR images: A comparative study," *Future Generation Computer Systems*, vol. 90, pp. 359–367, 2019, https://doi.org/10.1016/j.future.2018.08.008.

[37] K. Munir, H. Elahi, A. Ayub, F. Frezza, and A. Rizzi, "Cancer diagnosis using deep learning: A bibliographic review," *Cancers*, vol. 11, no. 9, p. 1235, 2019, https://doi.org/10.3390/cancers11091235.

[38] M. W. Nadeem, M. A. A. Ghamdi, M. Hussain, M. A. Khan, K. M. Khan, S. H. Almotiri, and S. A. Butt, "Brain tumor analysis empowered with deep learning: A review, taxonomy, and future challenges," *Brain Sciences*, vol. 10, no. 2, p. 118, 2020, https://doi.org/10.3390/brainsci10020118.

[39] S. Khawaldeh, U. Pervaiz, A. Rafiq, and R. S. Alkhawaldeh, "Noninvasive grading of glioma tumor using magnetic resonance imaging with convolutional neural networks," *Applied Sciences*, vol. 8, no. 1, p. 27, 2017, https://doi.org/10.3390/app8010027.

[40] A. M. Gab Allah, A. M. Sarhan, and N. M. Elshennawy, "Classification of brain MRI tumor images based on deep learning PGGAN augmentation," *Diagnostics*, vol. 11, no. 12, p. 2343, 2021, https://doi.org/10.3390/diagnostics11122343.

[41] M. Nickparvar, "Brain Tumor MRI Dataset," *Kaggle*, 2019, https://www.kaggle.com/datasets/masoudnickparvar/brain-tumor-mri-dataset.

[42] T.-H. Nguyen, T.-N. Nguyen, and B.-V. Ngo, "A VGG-19 model with transfer learning and image segmentation for classification of tomato leaf disease," *AgriEngineering*, vol. 4, no. 4, pp. 871–887, 2022, https://doi.org/10.3390/agriengineering4040056.

[43] T. Hussain, J. Hong, and J. Seok, "A hybrid deep learning and machine learning-based approach to classify defects in hot rolled steel strips for smart manufacturing," *Computers, Materials and Continua*, vol. 80, no. 2, pp. 2099–2119, 2024, https://doi.org/10.32604/cmc.2024.050884.

[44] S. Sathyanarayanan and B. R. Tantri, "Confusion matrix-based performance evaluation metrics," *African Journal of Biomedical Research*, vol. 27, no. 4S, pp. 4023–4031, 2024, https://doi.org/10.53555/AJBR.v27i4S.4345.

[45] G. Zeng, "Invariance properties and evaluation metrics derived from the confusion matrix in multiclass classification," *Mathematics*, vol. 13, no. 16, p. 2609, 2025, https://doi.org/10.3390/math13162609.

[46] O. Rainio, J. Teuho, and R. Klén, "Evaluation metrics and statistical tests for machine learning," *Scientific Reports*, vol. 14, no. 1, p. 6086, 2024, https://doi.org/10.1038/s41598-024-56706-x.

[47] M. A. Khan, I. Ashraf, M. Alhaisoni, R. Damaševičius, R. Scherer, A. Rehman, and S. A. C. Bukhari, "Multimodal brain tumor classification using deep learning and robust feature selection: A machine learning application for radiologists," *Diagnostics*, vol. 10, no. 8, p. 565, 2020, https://doi.org/10.3390/diagnostics10080565.

[48] M. Rasool, N. A. Ismail, W. Boulila, A. Ammar, H. Samma, W. M. S. Yafooz, and A.-H. M. Emara, "A hybrid deep learning model for brain tumour classification," *Entropy*, vol. 24, no. 6, p. 799, 2022, https://doi.org/10.3390/e24060799.

[49] W. A. K. Naser, E. A. Kadim, and S. H. Abbas, "SVM kernels comparison for brain tumor diagnosis using MRI," *Global Journal of Engineering and Technology Advances*, vol. 7, no. 2, pp. 26–36, 2021, https://doi.org/10.30574/gjeta.2021.7.2.0065.

[50] N. B. Bahadure, A. K. Ray, and H. P. Thethi, "Image analysis for MRI based brain tumor detection and feature extraction using biologically inspired BWT and SVM," *International Journal of Biomedical Imaging*, vol. 2017, p. 9749108, 2017, https://doi.org/10.1155/2017/9749108.

[51] Z. Rasheed, Y.-K. Ma, I. Ullah, M. Al-Khasawneh, S. S. Almutairi, and M. Abohashrh, "Integrating convolutional neural networks with attention mechanisms for magnetic resonance imaging-based classification of brain tumors," *Bioengineering*, vol. 11, no. 7, p. 701, 2024, https://doi.org/10.3390/bioengineering11070701.

[52] M. M. Musthafa, T. R. Mahesh, V. Vinoth Kumar, and S. Guluwadi, "Enhancing brain tumor detection in MRI images through explainable AI using Grad-CAM with ResNet50," *BMC Medical Imaging*, vol. 24, no. 1, p. 107, 2024, https://doi.org/10.1186/s12880-024-01292-7.